processes

MDPI

Article

Effect of Cambered and Oval-Grooved Roll on the Strain Distribution During the Flat Rolling Process of a Wire

Joong-Ki Hwang

School of Mechanical Engineering, Tongmyong University, Busan 48520, Korea; jkhwang@tu.ac.kr; Tel.: +82-51-629-1567

Received: 20 April 2020; Accepted: 15 July 2020; Published: 20 July 2020

Abstract: The effect of the roll design on the strain distribution of the flat surface, lateral spreading, and the strain inhomogeneity of a flat-rolled wire were investigated during the flat rolling process. Oval-grooved and cambered rolls with various radii were applied to the flat rolling process based on a numerical simulation. The effective strain on the flat surface of the wire increased when using a cambered roll due to the highly intensified contact pressure on the flat surface, while the effective strain on the flat surface of the wire decreased when using an oval-grooved roll. Lateral spreading decreased when using an oval-grooved roll because the spread in the free surface area of the wire was highly restricted by the oval-grooved roll shape. In contrast, the spread in the surface area increased when using a cambered roll due to the less-restricted metal flow at the free surface. Accordingly, a cambered roll with a small radius is highly recommended in order to improve the surface quality of flat-rolled wires. This is beneficial for industrial plants because the cambered roll can be easily applied in flat rolling plants.

Keywords: roll design; flat-rolled wire; strain inhomogeneity; normal pressure; macroscopic shear bands

1. Introduction

Flat-rolled wires are widely used in windshield wipers, springs, guide rails, and saw blades [1]. There are two main issues in the flat rolling of wire. The first issue is shape control of the flat-rolled wires, because direct shape control is impossible during the flat rolling of wire; that is, lateral spreading occurs in the free surface of the wire [2]. Consequently, several studies have been conducted regarding the influence of process conditions, such as reductions in the height, initial wire size, friction, and rolling speed on the lateral spreading of a wire using empirical or numerical methods [1–7]. The studies reported that the lateral spreading of a wire increased with reductions in the height and friction, which was independent of the rolling velocity. The second issue is the inhomogeneity of the mechanical properties of flat-rolled wires. In particular, the low hardness on the flat surfaces of a wire is a crucial issue in the industry. Therefore, the strain distribution of flat-rolled wire has been investigated using finite element (FE) analysis and hardness tests [8–14]. Kazeminezhad and Karimi Taheri [9] reported that the strain inhomogeneity of a wire increased with decreasing the reduction in height and increasing the friction coefficient. Vallellano et al. [12] reported that the maximum contact pressure occurred in the roll entry zone due to the local inhomogeneity of deformation. Hwang [14] reported that the difference of the effective strain along the horizontal direction was much higher than that of the vertical direction, and the maximum difference of the effective strain occurred in between the center area and the free surface area of the flat-rolled wire. It is well known that the occurrence of macroscopic shear bands (MSBs) is highly related to the strain inhomogeneity of flat-rolled wire [8], because the occurrence of MSBs indicates that the deformation is highly inhomogeneous during the

forming process. The occurrence of MSBs has been reported in several compression-type metal-forming processes, such as plain strain compression [15], uniaxial compression [16], flat rolling of wire [8], and flat roll drawing [17]. The restricted metal flow at the interface between the specimen and tool is the main reason for the occurrence of MSBs in specimens during the compression-type forming process. Therefore, the strain inhomogeneity can be improved by controlling the behavior of MSBs during the rolling process.

Over the past three decades, although several studies have reported the influence of process conditions on the strain inhomogeneity of flat-rolled wires [8–11], most of the studies have been conducted based on external process conditions, such as the roll diameter, reduction in thickness, rolling speed, and friction coefficient. Meanwhile, it may be inferred from experience that the roll shape is an important design parameter in shape rolling processes, such as caliber rolling [18,19] and flat rolling of wire. However, no studies have reported on the effect of the roll design on the strain distribution and shape control of a flat-rolled wire.

Therefore, the present study focuses on the effect of the roll design on the strain distribution in a flat-rolled wire in order to improve the homogeneity of mechanical properties and to increase the hardness on the flat surface of a wire. Oval-grooved roll and cambered roll techniques with various radii were applied to the flat rolling process based on numerical simulation, and then a general strategy for fabricating high-quality flat-rolled wire products was deduced, considering the process and working conditions in industries.

2. Numerical Procedures

The DEFORM FE commercial software developed by Scientific Forming Technologies Corporation in Ohio, USA, version 11.0 with a three-dimensional (3D) module was used to analyze the flat wire rolling process, because a flat-rolled wire experiences 3D inhomogeneous deformation during the process [14]. The workpiece was assumed to be an isotropic and rigid plastic material, while the effect of the strain rate was not considered in this study. In this case, the constitutive behavior was generally described by Hollomon's law [20,21], as follows:

$$\sigma = K\varepsilon^n \tag{1}$$

where K means the strength coefficient and n refers to the strain hardening exponent. The K and n values of the present material are chosen as 1980 and 0.54, respectively, based on the curve fitting of the tensile test in twinning-induced plasticity (TWIP) steel in [22]. Each value was inserted into the DEFORM commercial software model as follows:

$$\sigma = 1980\varepsilon^{0.54} \tag{2}$$

All rolls with 400 mm diameter were assumed to be rigid bodies. The rolling speed was set to 5 revolutions per minute (RPM) to ignore the effect of temperature rise. Oval-grooved rolls with radii of 10, 20, and 30 mm were applied to the flat rolling process to tailor the strain distribution, as shown in Figure 1b. A cambered roll was also applied with various radii to understand the effect of the roll shape on the strain distribution of a flat-rolled wire, as shown in Figure 1c. The oval-grooved roll and cambered roll were only used for the first rolling pass, while the same flat roll was applied to the second pass, as shown in Figure 1, to fabricate a flat-rolled wire with the desired shape for customers. The reduction in height (R_h) was calculated using the following equation:

$$R_h = \frac{h_0 - h_1}{h_0} \times 100(\%) \tag{3}$$

where h_0 and h_1 are the initial and final heights of the wire, respectively. R_h was about 22% at the first pass, regardless of the roll design. At the second pass, the R_h was approximately 18%, and thus the total R_h was 35%. The shear friction coefficient between the wire and the roll interface was selected as 0.3 [14].

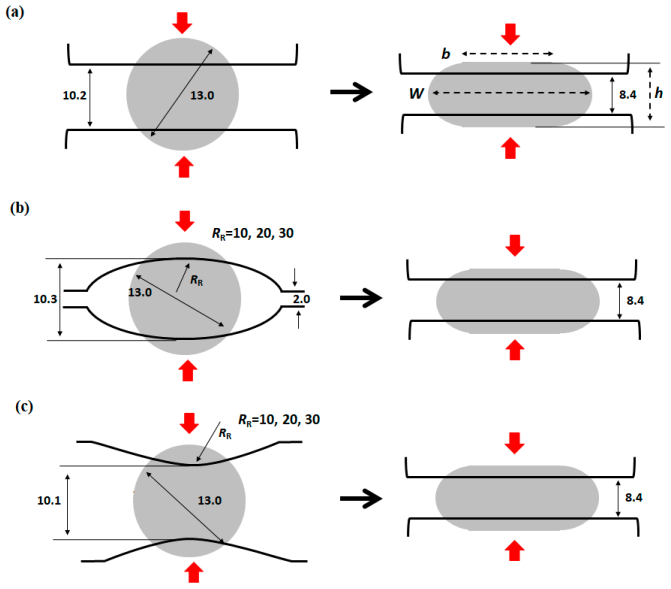

Figure 1. Schematic of the cross-sectional shape of the wire and the roll design during the flat rolling process with a (**a**) flat roll, (**b**) oval-grooved roll, and (**c**) cambered roll.

To reduce the computational cost, only one-quarter of the full geometry was calculated, owing to the symmetric condition of the flat-rolled wire. Approximately 15,000 brick-type elements were used, while 300 elements were used in the cross-section of the wire, as shown in Figure 2.

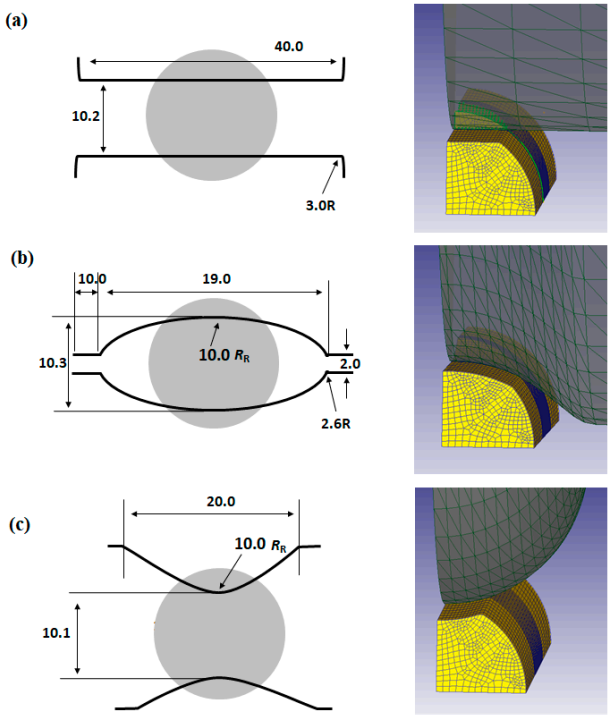

Figure 2. Detailed geometry and elements of the numerical modeling with a (**a**) flat roll, (**b**) oval-grooved roll with a radius of 10 mm, and (**c**) cambered roll with a radius of 10 mm.

3. Validation of the Numerical Model

The accuracy of the numerical model was validated prior to evaluating the results of the numerical simulation by comparing the numerically simulated geometries with the measured geometries of the flat-rolled TWIP steel wire. The analyzed chemical composition of TWIP steel is Fe-19.94Mn-0.60C-1.03Al (wt.%), which was fabricated by vacuum induction method. Prior to hot rolling, the ingot measuring 125 mm in thickness was homogenized at 1200 °C for 3 h. Then, the ingot was directly rolled onto a plate measuring 20 mm in thickness using multipass rolling at temperatures above 950 °C, followed by air cooling to simulate the hot rod rolling process. The hot-rolled plate was machined into several round bars with a diameter of 13 mm for the flat wire rolling test. The bar was rolled into the flat-rolled wire using flat rolls with a diameter of 400 mm at a rolling speed of 5 RPM. The other process conditions were kept the same as those of the numerical simulation.

Figure 3a shows the comparison of the cross-sectional shapes of flat-rolled wires based on the experimental and numerical simulation, as well as the used terminologies in this study, while Figure 3b compares the measured and numerically simulated width of the contact area (b) and the lateral spread (W) values with the total R_h. As expected, the W and b values increased when increasing the total R_h. Overall, the W and b values obtained by the numerical simulation were in good agreement with the experimental values. However, it was found that the deviation of the W value between the two results slightly increased with the total R_h. This inconsistency was related to the hardening model applied in this study [5] and the selected friction coefficient of 0.3.

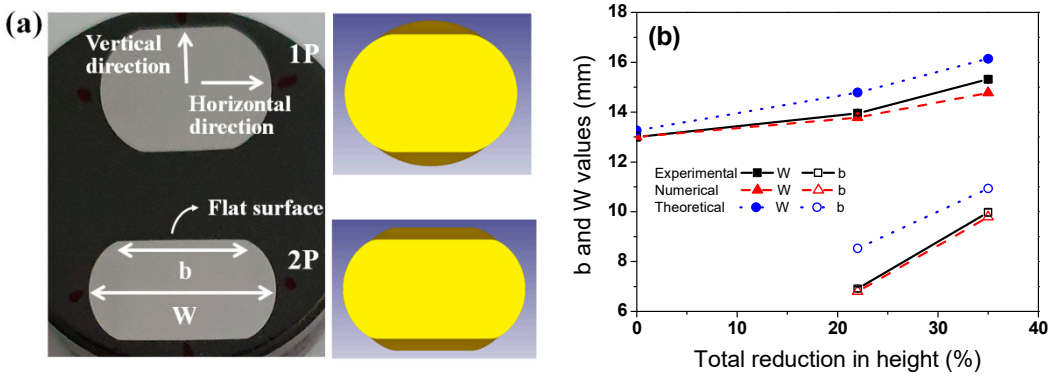

Figure 3. (**a**) Photograph of the caliber-rolled TWIP steel wire in this experiment and the shape of the deformed wire based on the numerical simulation. (**b**) Comparison of the measured, simulated, theoretically derived W and b values as a function of the total reduction in height.

Meanwhile, Kazeminezhad and Karimi Taheri [1,3] suggested the prediction of b and W values as a function of the total reduction in the height (Δh), h_0, and h_1 from the plain carbon steels as the following equations:

$$b = \sqrt{2\Delta h h_0} \tag{4}$$

$$\frac{W_1}{W_0} = 1.02\left(\frac{h_0}{h_1}\right)^{0.45} \tag{5}$$

where the subscripts of 0 and 1 indicate the initial and final values during the flat rolling process, respectively. As shown in Figure 3b, the W and b values of TWIP steel were lower compared to those of the plain carbon steel theoretically suggested in the relationships. Hwang [14] suggested that this result is highly related to the different strain hardening behavior between plain carbon steels and TWIP steel. Namely, the strain hardening exponents of TWIP steel are much higher than those of plain carbon steels [23]. Overall, it can be concluded from an engineering application point of view that the proposed FE analysis for the flat wire rolling process can be used to evaluate the characteristics of the shape and strain distribution with the process conditions.

4. Results and Discussion

4.1. Strain Distribution with Roll Design

Figure 4 shows a comparison of the contours of the von Mises strain (effective strain) and normal pressure of the flat-rolled wire with the representative roll designs (i.e., flat roll design, oval-grooved and cambered rolls with a radius of 10 mm). Clearly, the strain distribution in the flat-rolled wire was complex—it had two MSBs with high effective strain [8]. The center area tended to have a maximum strain, while the free surface area tended to have a minimum strain. However, the distribution of the effective strain of the wire was different with the roll design. In particular, the shapes of the MSBs changed with the roll design. During the first pass, the total width of the MSBs increased with the oval-grooved roll, while that of the MSBs decreased with the cambered roll. The different behavior of MSBs with the roll design was related to the normal pressure on the wire surface [24,25], as shown in Figure 4, indicating that the MSBs can be controlled by tailoring the contact pressure on the specimen during the rolling process. It should be noted that it is necessary to increase the strength on the flat surface of a wire, because the external stress was mainly imposed on the flat surface of the wires under service. For a better understanding of the strain distribution of the flat-rolled wire, the effective strain was extracted from the contour maps in both the cross-section and the flat surface, as shown in Figure 5 for the final product (i.e., after the second pass). The maximum effective strain in the center area decreased with the cambered roll, whereas it increased with the oval-grooved roll. Meanwhile, the minimum effective strain in the free surface area was similar regardless of the roll design, indicating that the cambered roll reduced the overall strain inhomogeneity of the flat-rolled wire.

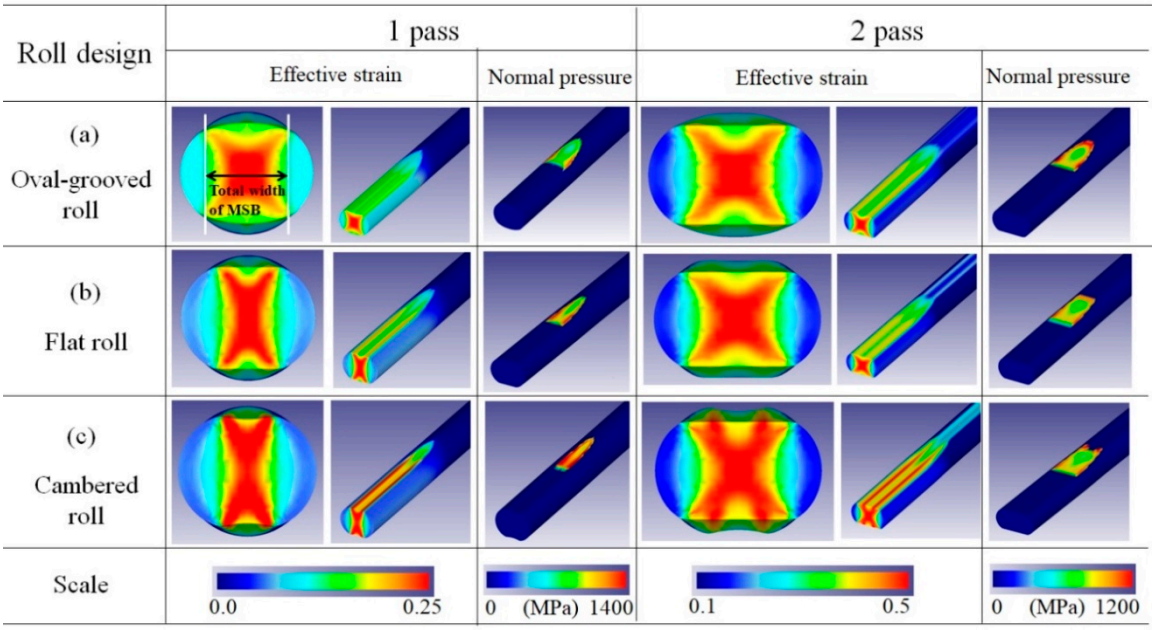

Figure 4. Contour maps of the effective strain and normal pressure of flat-rolled wires with a roll design and pass.

Interestingly, the effective strain on the flat surface of the wire increased when using the cambered roll, as shown in Figure 5c, whereas the oval-grooved roll decreased the effective strain on the flat surface of the wire. To deduce a general conclusion, a new non-dimensional indicator for the roll design (I_{RD}) was defined as follows:

$$I_{RD} = \frac{D_{wire}}{R_R} \tag{6}$$

where R_R and D_{wire} are the surface radius of the roll (Figure 1) and the diameter of the initial round wire (13 mm), respectively. To calculate the R_R value, the surface radius of the cambered roll was taken to be

negative due to the reverse roll shape compared to the oval-grooved roll, as listed in Table 1. Figure 6a shows the maximum and minimum effective strains in the cross-section of the flat-rolled wire at the second pass. The maximum strain at the center area of the wire slightly increased with I_{RD}, meaning that the maximum strain increased with the decrease in the radius of the oval-grooved roll. In other words, the oval-grooved roll increased the stress concentration at the center area of the specimen due to the restriction of the plastic deformation according to roll shape, as compared to the flat and cambered rolls, as shown in Figure 2. In addition, it is well known that the strain is highly concentrated in the center area during bar and rod rolling with the oval-round roll pass sequence [26–28]. The minimum effective strain had a constant value with I_{RD}, indicating that the oval-grooved roll and camber roll did not affect the level of strain in the free surface area of a wire. In summary, the cambered roll slightly reduced the strain inhomogeneity of the specimen during the flat rolling process.

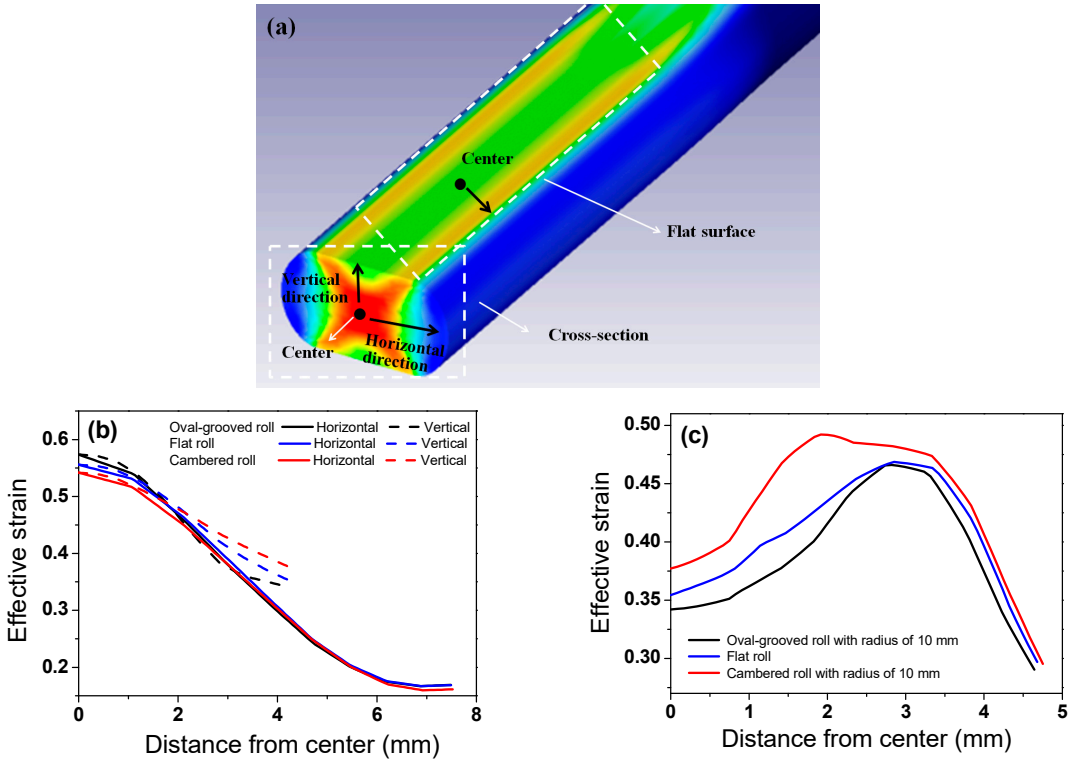

Figure 5. (**a**) Schematic showing the terminologies used in this study. Comparison of the effective strain profiles in (**b**) cross-sections of flat-rolled wires along the horizontal and vertical directions, and (**c**) the flat surface of a flat-rolled wire with the representative roll design.

Table 1. Comparison of the seven roll designs and related values during the flat rolling process used in this study.

Roll Design	Values		
	Surface Radius (mm)	R_R	I_{RD}
Oval-grooved roll	10	10	1.3
	20	20	0.65
	30	30	0.43
Flat roll	∞	∞	0
Cambered roll	30	−30	−0.43
	20	−20	−0.65
	10	−10	−1.3

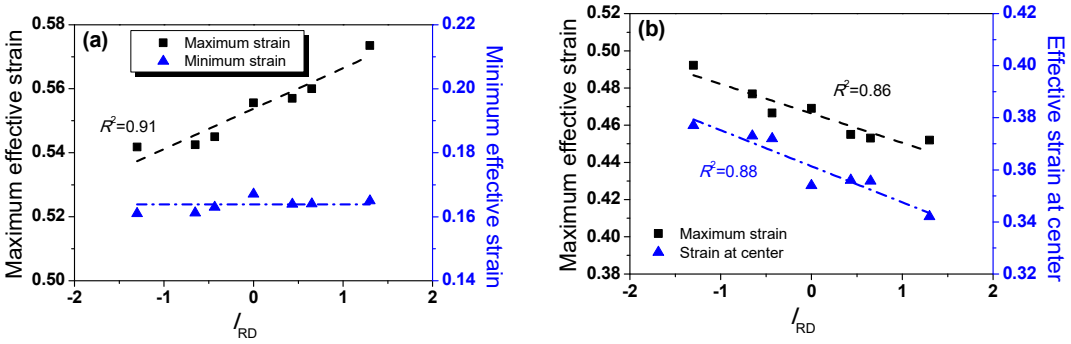

Figure 6. Variations in (**a**) the maximum and minimum effective strains in the cross-sections of the flat-rolled wires and (**b**) the maximum and centered effective strains on the flat surface of a wire with I_{RD}.

The maximum effective strain on the flat surface of the wire decreased with I_{RD}, as shown in Figure 6b, meaning that the camber roll with the small radius increased the strength on the flat surface of the wire. This was due to the strong concentration of the normal pressure on the wire surface, as shown in Figure 4c. Namely, the strain distribution on the flat surface of the wire was highly dependent on the normal contact pressure. Based on a similar mechanism, the strain of the center area on the flat surface of the wire was improved when using the cambered roll with a small radius. This result is attractive for industrial plants because many process designers want to improve the hardness of the flat surfaces in a wire owing to the strict customer demands.

4.2. Shape of Flat-Rolled Wire with Roll Design

To apply the shaped rolls to the flat rolling process, the effect of the roll design on the shape of the final product needs to be considered. Figure 7 shows the variation in b and W values with I_{RD} after the second pass. Both values decreased linearly with I_{RD}, indicating that the lateral spreading of the wire decreased when using the oval-grooved roll with a small radius, because the spreading in the free surface area of the wire was highly restricted by the roll shape and curvature, as shown in Figure 1b. In contrast, the spreading in the surface area increased during the rolling process with the cambered roll due to the reduced restriction of the metal flow in the free surface area, as shown in Figure 1c. These results practically imply that the size of the initial wire needs to be changed when using the shaped roll during the flat rolling of wire due to the different wire spreading results with roll designs.

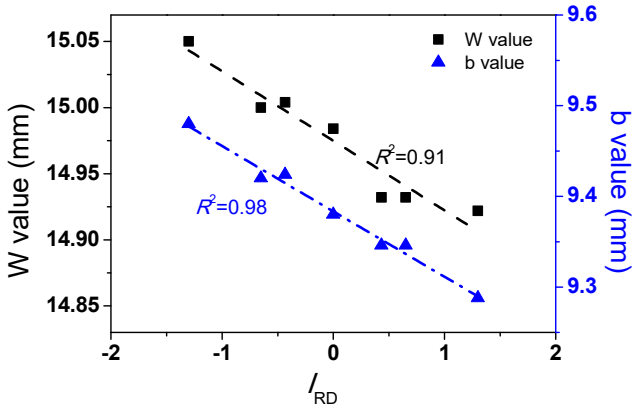

Figure 7. Variations in the b and W values with I_{RD}.

4.3. Design Concept for a High-Quality Flat-Rolled Wire

To make high-quality flat-rolled wires, a practical strategy was designed, as shown in Figure 8, based on the results achieved in the above comparative study. The strain on the flat surface of the wire

increased with decreasing I_{RD}, while the strain inhomogeneity in the cross-section of the wire was slightly reduced with decreasing I_{RD}, meaning that we can produce higher quality flat-rolled wire products using a cambered roll with a small radius. In contrast, the use of an oval-grooved roll is not a good idea when fabricating a flat-rolled wire. The proposed design concepts can provide process designers with seeding ideas to choose the optimal process conditions for high-quality flat-rolled wires. This is beneficial for industrial plants because a cambered roll can be easily applied in flat rolling plants. It is worth noting that the proposed practical strategy was valid for most materials, since it was derived from the general plastic forming conditions. However, the effects of the kinematic hardening, the strain rate sensitivity in the material, and the friction coefficient should be considered to obtain more reliable results. In addition, it should be noted that the effects of the roll design on the b and W values should be considered to obtain a wire with accurate dimensions and tolerance (Figure 7). For mass production, the wear issue needs to be considered when applying the cambered roll in the flat rolling of wire. Additionally, the present results need to be confirmed by experimental data, such as a hardness analysis and microstructure evolution data. In this respect, additional research is necessary.

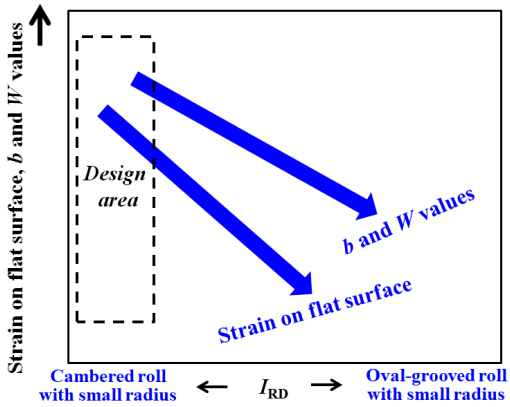

Figure 8. Schematic description of the effective strain on the flat surface and shape of a flat-rolled wire with I_{RD}.

5. Conclusions

The effect of the roll design on the strain distribution of the flat surface and on b, and W values; and the strain inhomogeneity of flat-rolled wires were systematically investigated during the flat rolling process. The major conclusions are as follows:

1. The effective strain on the flat surface of the wire increased when using a cambered roll due to the highly intensified contact pressure, while the effective strain on the flat surface of the wire decreased when using an oval-grooved roll;
2. The b and W values decreased when using an oval-grooved roll with a small radius because the spread in the free surface area of the wire was highly restricted by the roll shape. In contrast, the spread in the surface area increased when using a cambered roll due to the less-restricted metal flow at the free surface;
3. A new practical strategy was proposed for fabricating high-quality flat-rolled wires. A cambered roll with a small radius can improve the surface quality of flat-rolled wires. This is beneficial for industrial plants because cambered rolls can be applied easily in flat rolling plants.

Funding: This work was supported by the National Research Foundation of Korea (NRF) grant funded by the Korea government (MSIT) (NRF-2018R1D1A1B07050103).

Conflicts of Interest: The author declares no conflicts of interest.

References

1. Kazeminezhad, M.; Karimi Taheri, A. A theoretical and experimental investigation on wire flat rolling process using deformation pattern. *Mater. Des.* **2005**, *26*, 99–103. [CrossRef]
2. Kobayashi, K.; Asakawa, M.; Kobayashi, M. Deformation behavior of round wire in compression using a cylindrical tool and the analysis of width spreading in flat rolling. *Wire J. Int.* **2005**, *38*, 74–79.
3. Kazeminezhad, M.; Taheri, A.K. An experimental investigation on the deformation behavior during wire flat rolling process. *J. Mater. Process. Technol.* **2005**, *160*, 313–320. [CrossRef]
4. Kazeminezhad, M.; Taheri, A.K.; Tieu, A.K. A study on the cross-sectional profile of flat rolled wire. *J. Mater. Process. Technol.* **2008**, *200*, 325–330. [CrossRef]
5. Massé, T.; Chastel, Y.; Montmitonnet, P.; Bobadilla, C.; Persem, N.; Foissey, S. Impact of mechanical anisotropy on the geometry of flat-rolled fully pearlitic steel wires. *J. Mater. Process. Technol.* **2011**, *211*, 103–112. [CrossRef]
6. Utsunomiya, H.; Hartley, P.; Pillinger, I. Three-Dimensional Elastic-Plastic Finite-Element Analysis of the Flattening of Wire Between Plain Rolls*. *J. Manuf. Sci. Eng.* **2000**, *123*, 397–404. [CrossRef]
7. Parvizi, A.; Pasoodeh, B.; Abrinia, K.; Akbari, H. Analysis of curvature and width of the contact area in asymmetrical rolling of wire. *J. Manuf. Process.* **2015**, *20*, 245–249. [CrossRef]
8. Kazeminezhad, M.; Taheri, A.K. The prediction of macroscopic shear bands in flat rolled wire using the finite and slab element method. *Mater. Lett.* **2006**, *60*, 3265–3268. [CrossRef]
9. Kazeminezhad, M.; Taheri, A.K. Deformation inhomogeneity in flattened copper wire. *Mater. Des.* **2007**, *28*, 2047–2053. [CrossRef]
10. Kazeminezhad, M.; Taheri, A.K. The effect of 3D and 2D deformations on flattened wires. *J. Mater. Process. Technol.* **2008**, *202*, 553–558. [CrossRef]
11. Massé, T.; Chastel, Y.; Montmitonnet, P.; Bobadilla, C.; Persem, N.; Foissey, S. Mechanical and damage analysis along a flat-rolled wire cold forming schedule. *Int. J. Mater. Form.* **2011**, *5*, 129–146. [CrossRef]
12. Vallellano, C.; Cabanillas, P.; García-Lomas, F. Analysis of deformations and stresses in flat rolling of wire. *J. Mater. Process. Technol.* **2008**, *195*, 63–71. [CrossRef]
13. Iankov, R. Finite element simulation of profile rolling of wire. *J. Mater. Process. Technol.* **2003**, *142*, 355–361. [CrossRef]
14. Hwang, J.-K. Deformation Behaviors of Flat Rolled Wire in Twinning-Induced Plasticity Steel. *Met. Mater. Int.* **2019**, *26*, 603–616. [CrossRef]
15. Paul, H.; Driver, J.; Tarasek, A.; Wajda, W.; Miszczyk, M. Mechanism of macroscopic shear band formation in plane strain compressed fine-grained aluminium. *Mater. Sci. Eng. A* **2015**, *642*, 167–180. [CrossRef]
16. Eom, J.; Son, Y.; Jeong, S.; Ahn, S.; Jang, S.; Yoon, D.; Joun, M. Effect of strain hardening capability on plastic deformation behaviors of material during metal forming. *Mater. Des.* **2014**, *54*, 1010–1018. [CrossRef]
17. Lambiase, F.; Di Ilio, A. Deformation inhomogeneity in roll drawing process. *J. Manuf. Process.* **2012**, *14*, 208–215. [CrossRef]
18. Inoue, T. Optimum pass design of bar rolling for production bulk ultrafine-grained steel by numerical simulation. *Mat. Sci. Forum* **2010**, *654–656*, 1561–1564. [CrossRef]
19. Hwang, J.-K.; Kim, S.J. Effect of reduction in area per pass on strain distribution and microstructure during caliber rolling in twinning-induced plasticity steel. *J. Iron Steel Res. Int.* **2019**, *27*, 62–74. [CrossRef]
20. Choung, J.; Cho, S.R. Study on true stress correction from tensile tests. *J. Mech. Sci. Technol.* **2008**, *22*, 1039–1051. [CrossRef]
21. Koc, P.; Štok, B. Computer-aided identification of the yield curve of a sheet metal after onset of necking. *Comput. Mater. Sci.* **2004**, *31*, 155–168. [CrossRef]
22. Hwang, J.-K.; Yi, I.-C.; Son, I.-H.; Yoo, J.-Y.; Kim, B.; Zargaran, A.; Kim, N.J. Microstructural evolution and deformation behavior of twinning-induced plasticity (TWIP) steel during wire drawing. *Mater. Sci. Eng. A* **2015**, *644*, 41–52. [CrossRef]
23. Hwang, J.-K. The microstructure dependence of drawability in ferritic, pearlitic, and TWIP steels during wire drawing. *J. Mater. Sci.* **2019**, *54*, 8743–8759. [CrossRef]
24. Carlsson, B. The contact pressure distribution in flat rolling of wire. *J. Mater. Process. Technol.* **1998**, *73*, 1–6. [CrossRef]

25. Kazeminezhad, M.; Taheri, A.K. Calculation of the rolling pressure distribution and force in wire flat rolling process. *J. Mater. Process. Technol.* **2006**, *171*, 253–258. [CrossRef]
26. Kwon, H.-C.; Lee, Y.; Im, Y. Experimental and Numerical Prediction of Austenite Grain Size Distribution in Round-oval Shape Rolling. *ISIJ Int.* **2003**, *43*, 1967–1975. [CrossRef]
27. Jung, K.; Lee, H.W.; Im, Y.-T. A microstructure evolution model for numerical prediction of austenite grain size distribution. *Int. J. Mech. Sci.* **2010**, *52*, 1136–1144. [CrossRef]
28. Hwang, J.-K. Effects of caliber rolling on microstructure and mechanical properties in twinning-induced plasticity (TWIP) steel. *Mater. Sci. Eng. A* **2018**, *711*, 156–164. [CrossRef]